Finite correlation length scaling with infinite projected entangled pair states at finite temperature

Czarnik, P.; Corboz, P.

DOI
10.1103/PhysRevB.99.245107

Publication date
2019

Document Version
Final published version

Published in
Physical Review B

Finite correlation length scaling with infinite projected entangled pair states at finite temperature

Piotr Czarnik[1] and Philippe Corboz[2]

[1]*Institute of Nuclear Physics, Polish Academy of Sciences, Radzikowskiego 152, PL-31342 Kraków, Poland*

[2]*Institute for Theoretical Physics and Delta Institute for Theoretical Physics, University of Amsterdam, Science Park 904, 1098 XH Amsterdam, The Netherlands*

(Received 11 April 2019; revised manuscript received 24 May 2019; published 6 June 2019)

We study second-order finite-temperature phase transitions of the two-dimensional quantum Ising and interacting honeycomb fermion models using infinite projected entangled pair states (iPEPS). We obtain an iPEPS thermal state representation by variational tensor network renormalization. We find that at the critical temperature T_c the iPEPS correlation length is finite for the computationally accessible values of the iPEPS bond dimension D. Motivated by this observation, we investigate the application of finite correlation length scaling (FCLS), which has been previously used for iPEPS simulations of quantum critical points at $T = 0$, to obtain precise values of T_c and the universal critical exponents. We find that in the vicinity of T_c the behavior of observables follows well the one predicted by FCLS. Using FCLS we obtain T_c and the critical exponents in agreement with quantum Monte Carlo results except for couplings close to the quantum critical points where larger bond dimensions are required.

DOI: 10.1103/PhysRevB.99.245107

I. INTRODUCTION

Tensor networks [1–5] are representations of weakly entangled states obeying an area law of entanglement [6–8]. They are a basis for variational numerical methods for strongly correlated quantum many-body systems, enabling simulations of fermionic, bosonic, and spin models with the same leading computational complexity [9–14]. The powerful density matrix renormalization group (DMRG) [15,16] approximates a state of a system by a one-dimensional (1D) tensor network called matrix product state (MPS) [17–19]. Two-dimensional (2D) projected entangled pair states (PEPS) [20], called also tensor product states [21,22], were initially applied as a variational *Ansatz* for 2D ground states [12,14,23–25] bringing new insights into paradigmatic models of strongly correlated systems (see, e.g., [26–32]). Recent years brought new applications of PEPS [33–37] and further progress in the fields of numerical optimization [38–41] and contraction [42,43] of PEPS.

Thermal states of 2D local Hamiltonians obey an area law for mutual information, which is reproduced by projected entangled pair operators (iPEPO) representing thermal states and infinite projected entangled pair states (iPEPS) representing purifications of thermal states [44], giving motivation to use iPEPS for thermal state simulations [45,46]. Recently, new methods for simulation of thermal states, based on iPEPS and iPEPO, were proposed [36,47–50]. Recent years brought also developments in the field of the closely related direct contraction methods for three-dimensional (3D) tensor networks representing partition functions of 2D quantum models [51–55] and MPS/MPO based simulations of thermal states of finite-width cylinders [56,57]. Some of those methods were already applied to challenging problems [58–62].

Among demanding problems in the field of 2D strongly correlated systems are finite-temperature critical phenomena and in particular finite-temperature second-order phase transitions. Some of the methods mentioned above were already applied to investigate 2D critical phenomena based on the assumption that large enough D can be obtained to provide results which are converged in D [36,58,59,61], however, for more challenging cases reaching convergence in D will in general be difficult.

Here, we demonstrate that even in the case when convergence in D cannot be obtained, it is possible to take finite-D effects systematically into account using a finite correlation length scaling (FCLS) [63–66]. Furthermore, we show that FCLS can be used to obtain critical data for a finite-temperature phase transition, i.e., the critical temperature T_c and the universal critical exponents.

FCLS, originally called finite entanglement scaling (FES), was first proposed to investigate 1D quantum critical points by infinite MPS (iMPS) [63,64,67]. These critical points violate the area law of entanglement [68] and as such cannot be represented by finite-D iMPS, which have a finite correlation length ξ_D. It was shown that in the case of the optimal iMPS finite-D ground-state approximation, the finite D modifies observables of the critical state as if the system was finite with the size proportional to ξ_D [63,64]. It was also shown that the scaling of the observables with increasing ξ_D can be used to determine the critical exponents and the precise location of the critical point similarly as in standard finite-size scaling for quantum Monte Carlo (QMC) simulations [63,64,67].

A similar idea was applied earlier in corner transfer matrix renormalization group (CTMRG) simulations of 2D critical thermal states of classical models. CTMRG approximately contracts a 2D tensor network representing a partition function of a 2D classical system. The approximation introduces an effective correlation length controlled by a refinement parameter χ of the method [69]. A scaling *Ansatz* assuming that this correlation length is proportional to the effective

system size was introduced to find the critical properties [69].

FCLS was recently applied to iPEPS simulations of 2D Lorentz-invariant quantum critical points, i.e., quantum critical points with a linear dispersion relation of low-energy excitations [65,66]. It was shown that in such case the optimal finite-D iPEPS approximating a critical ground state has a finite correlation length ξ_D, and that FCLS can be used to determine the critical coupling and the universal critical exponents.

In this paper, we simulate second-order finite-temperature phase transitions for a 2D quantum Ising model and interacting spinless fermions on a honeycomb lattice using variational tensor network renormlization (VTNR) [47,48]. For thermal states at finite T we can expect that the exact state can be represented with a finite bond dimension D_{exact} [65]. Here, we find that at the critical temperature the obtained thermal states have a finite correlation length ξ_D for all bond dimensions used in this work, suggesting that we are in a regime where $D < D_{\text{exact}}$. This motivates us to investigate the possibility to use FCLS also in these cases. In this paper we present benchmark results demonstrating that indeed FCLS can be applied to determine the critical data.

This paper is organized as follows: In Sec. II we introduce a thermal state's representation by a purification and in Sec. III we describe how to represent such a purification using an iPEPS. In Sec. IV we introduce VTNR which we use to obtain the purification's iPEPS representation. In Sec. V we describe the CTMRG method which allows us to efficiently contract a 2D tensor network. In Sec. VI we explain how to determine the correlation length of an iPEPS using CTMRG. In Sec. VII we introduce FCLS and in Sec. VIII we describe how to determine the critical temperature T_c for a second-order phase transition using FCLS. In Secs. IX and X we present the benchmark results for the application of FCLS to simulations of thermal second-order phase transitions in the quantum Ising and interacting honeycomb fermions models, respectively. Finally, we provide our conclusions in Sec. XI.

II. PURIFICATIONS OF THERMAL STATES

A thermal state of a Hamiltonian H for temperature T is given by its thermal density matrix

$$\rho(T) = \frac{1}{Z(T)} e^{-H/T}, \quad Z(T) = \mathrm{Tr}\, e^{-H/T}. \tag{1}$$

Here, we consider lattice models for which the Hilbert space $\mathcal{H}$ is a tensor product of Hilbert spaces of individual lattice sites $\mathcal{H}_i$ spanned by states $\{|s_i\rangle,\ s_i = 1 \ldots d\}$.

We represent $\rho(T)$ by its purification $|\Psi(T)\rangle$ which is a pure state in an enlarged Hilbert space $\tilde{\mathcal{H}}$ created by introducing ancillary degrees of freedom. $\tilde{\mathcal{H}}$ is a tensor product of enlarged Hilbert spaces of individual sites $\tilde{\mathcal{H}}_i$, which are spanned by states $\{|s_i, a_i\rangle,\ s_i = 1 \ldots d,\ a_i = 1 \ldots d\}$ with an index a_i numbering the ancillary degrees of freedom. To obtain $\rho(T)$ from $|\psi(T)\rangle$ one needs to trace out the ancillary degrees of freedom

$$\rho(T) = \mathrm{Tr}_a |\Psi(T)\rangle\langle\Psi(T)|. \tag{2}$$

For $T = \infty$ we have

$$|\Psi(T=\infty)\rangle \propto \bigotimes_i \left(\sum_{s_i=1\ldots d} |s_i s_i\rangle \right), \tag{3}$$

and for finite T, $|\Psi(T)\rangle$ is obtained by an action of $e^{-H/(2T)}$ on the physical degrees of freedom of $|\Psi(T=\infty)\rangle$:

$$|\Psi(T)\rangle \propto e^{-H/(2T)} |\Psi(T=\infty)\rangle. \tag{4}$$

III. IPEPS REPRESENTATION OF THERMAL STATES

A projected entangled pair state state (PEPS) [20], also called a tensor product state [21,22], is a 2D tensor network representing a state obeying the area law of entanglement. In the simplest case, a PEPS represents a pure state and is built from a network of rank-5 tensors on a square lattice, with one tensor per lattice site. Each tensor has a physical index representing the local Hilbert space of a site. The other four indices of a tensor, called the virtual indices, are contracted with the virtual indices of the neighboring tensors. Their dimension is called the bond dimension D which controls the accuracy of the *Ansatz*. With growing D states with stronger entanglement can be represented by the PEPS. An infinite projected entangled pair state (iPEPS) is a PEPS representing a state on an infinite lattice. To obtain an iPEPS we introduce a unit cell of tensors which is periodically repeated on the lattice, i.e., the iPEPS is translational invariant by shifts of the unit-cell size. With each site in the unit cell we associate a different PEPS tensor. In this work we use a unit cell with two tensors A and B arranged in a checkerboard pattern (all states studied in this work are compatible with this unit cell).

As $|\Psi(T)\rangle$ is a pure state in the extended Hilbert space, it can be represented by an iPEPS with the tensors having an additional index for the ancillary degrees of freedom [see Figs. 1(a) and 1(b)]. Then, $\rho(T)$ (2) can be obtained by a contraction of the iPEPS representation of $|\Psi(T)\rangle$ and its Hermitian conjugate [see Fig. 1(c)].

The state at infinite temperature, $|\Psi(T=\infty)\rangle$, can be represented exactly by an iPEPS with the bond dimension $D = 1$, i.e., a product state (3). For finite T, $|\Psi(T)\rangle$ is obtained by an action of an operator $e^{-H/(2T)}$ on the physical degrees of freedom of $|\Psi(T=\infty)\rangle$ [Eq. (4)]. As $e^{-H/(2T)}$ in general does not have a numerically tractable exact tensor network representation, we use its Suzuki-Trotter decomposition [70–72] and VTNR [47,48] to find an iPEPS approximating $|\Psi(T)\rangle$ for a given bond dimension D.

IV. VTNR

We treat an operator $e^{-H/(2T)}$ as an imaginary-time evolution operator $e^{-\tau H}$ with the imaginary time $\tau = 1/(2T)$. We decompose H into a sum of classical Hamiltonians H_{cl}^j, i.e., Hamiltonians which are sums of commuting terms,

$$H = \sum_{j=1,\ldots,m} H_{cl}^j.$$

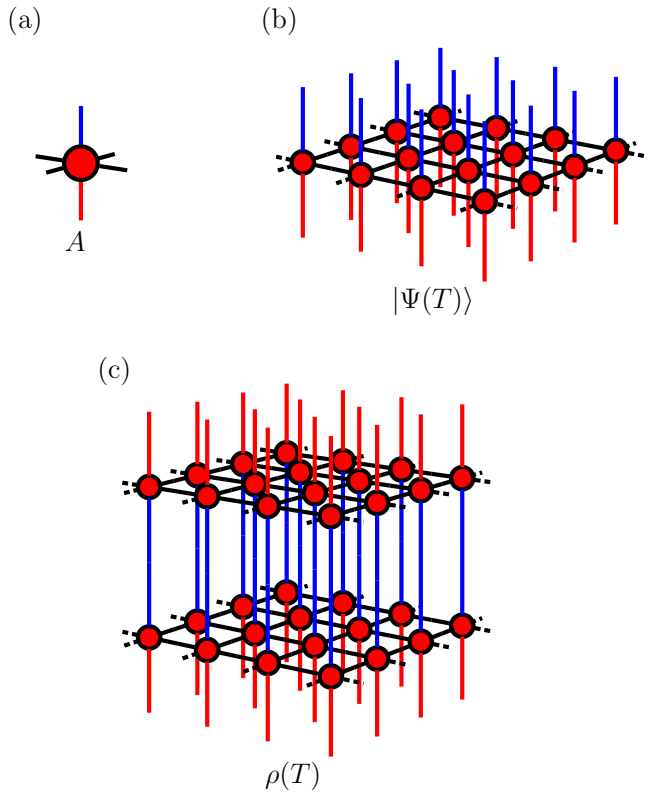

FIG. 1. In (a) a rank-6 PEPS tensor A for an iPEPS representation of a thermal state's purification $|\Psi(T)\rangle$. Each leg corresponds to an index of the tensor. The black indices are virtual indices with bond dimension D. The red index numbers physical degrees of freedom and the blue index numbers ancillary degrees of freedom. In (b) the iPEPS representation of $|\Psi(T)\rangle$ is built of copies of A whose virtual indices were contracted. Here, we show the case of a translationally invariant $|\Psi(T)\rangle$. The dashed black lines indicate that only a part of the infinite tensor network is shown. In (c) $\rho(T)$ is given by a contraction of the ancillary indices of the iPEPS representing $|\Psi(T)\rangle$ (the lower one) and its Hermitian conjugate $\langle\Psi(T)|$ (the upper one).

We use a second-order Suzuki-Trotter decomposition [70–72] to approximate $e^{-\tau H}$:

$$e^{-\tau H} = \Big(e^{-\delta\tau/2H_{cl}^{1}} \dots e^{-\delta\tau/2H_{cl}^{m-1}} e^{-\delta\tau H_{cl}^{m}} \times e^{-\delta\tau/2H_{cl}^{m-1}} \dots e^{-\delta\tau/2H_{cl}^{1}}\Big)^{\tau/\delta\tau} + O(\delta\tau^2). \quad (5)$$

The accuracy of the decomposition (5) is controlled by the size of the small time step $\delta\tau$. An exact iPEPO representation of an exponential of a classical Hamiltonian with a finite range of interaction can be found analytically and has $D = d^2$ at most (see Ref. [44] and simple examples in Refs. [47,48]). Using the Suzuki-Trotter decomposition (5) and iPEPO representations of the exponentials of H_{cl}^{j}, we approximate $|\Psi(T)\rangle$ [Eq. (4)] by the 3D tensor network shown in Fig. 2(a).

We use VTNR to approximate the 3D tensor network by an iPEPS with a numerically tractable bond dimension D, which yields an approximate representation of $|\Psi(T)\rangle$. In VTNR the iPEPS tensors are obtained by acting with tree tensor networks consisting of isometries [73] on the virtual indices of the 3D tensor network, as shown in Fig. 2(b). The isometries are found by a variational update to minimally distort the partition

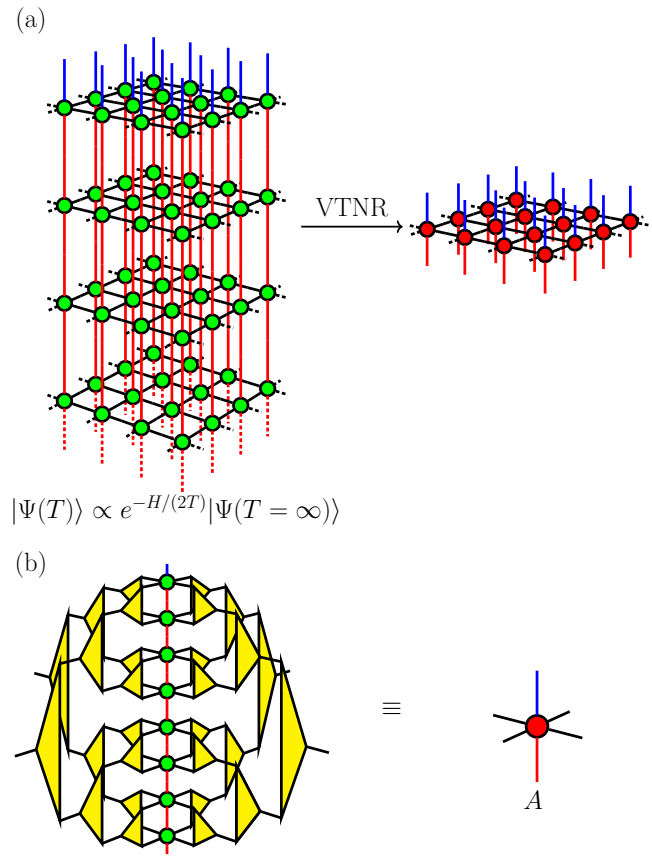

FIG. 2. In (a) at the left a 3D tensor network approximating $|\Psi(T)\rangle \propto e^{-H/(2T)}|\Psi(T=\infty)\rangle$ obtained by a Suzuki-Trotter decomposition (5) is shown. The top layer of the tensor network is an iPEPS with $D = 1$ representing $|\Psi(T=\infty)\rangle$ [Eq. (3)]. The lower layers are iPEPO representations of the exponentials of classical Hamiltonians appearing in the Suzuki-Trotter decomposition (5) of the $e^{-H/(2T)}$ operator, which acts on the physical indices (the red ones) of $|\Psi(T=\infty)\rangle$. VTNR approximates the 3D network by an iPEPS with the numerically tractable D shown at the right. Here, we show the case of a translationally invariant $|\Psi(T)\rangle$. In (b) the PEPS tensor A is obtained by VTNR from tensors of the 3D tensor network. Tree tensor networks of isometries (the yellow ones) are applied to virtual indices (the black ones) of the 3D tensor network giving A. Here, we show the case of the 3D network built from eight layers.

function $Z(T)$ as described in detail in Refs. [47,48]. The accuracy of the final iPEPS is controlled systematically by the bond dimension of the isometries, which here equals the bond dimension of the final iPEPS.

V. CORNER TRANSFER MATRIX RENORMALIZATION GROUP (CTMRG)

To compute expectation values of observables and the correlation length ξ, we use CTMRG [26,74–76]. CTMRG approximates contractions of an infinite number of copies of the PEPS tensors by contractions of a finite number of environment tensors C, E, where the accuracy is systematically controlled by the bond dimension χ of the environment tensors. An example of such an approximation is shown in

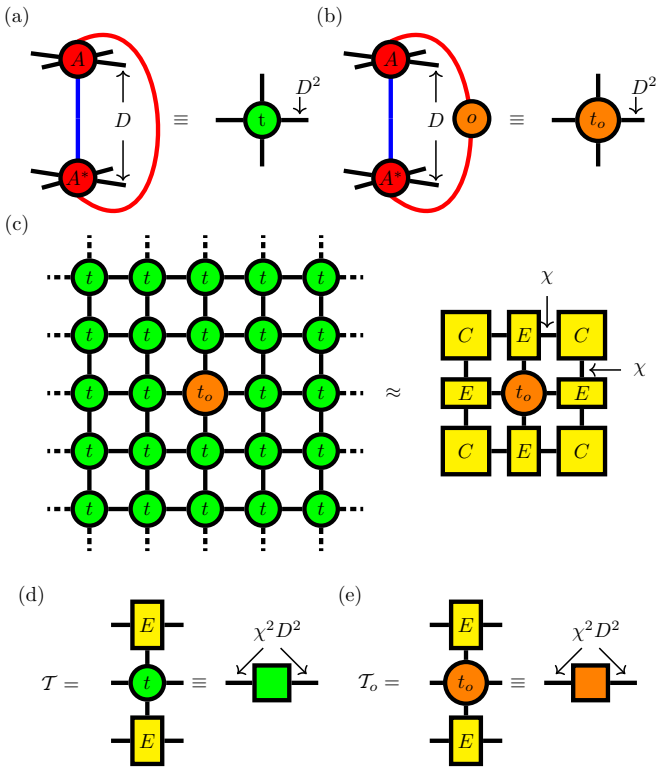

FIG. 3. In (a) physical (blue) and ancillary (red) indices of a PEPS tensor A and its complex conjugate A^* are contracted to create a tensor t. Furthermore, each pair of corresponding virtual indices of the contracted tensors, which have bond dimension D, is treated as a virtual index of the tensor t with bond dimension D^2. In (b) a tensor t_o is created analogously to t for a site at which an operator o is acting. In (c) the diagram used to compute an expectation value of o by the corner transfer matrix renormalization group (CTMRG) is shown. CTMRG approximates the infinite tensor network shown on the left by a contraction of a finite tensor network of tensors C, E, and t_o. The accuracy of the approximate contraction is systematically controlled by the bond dimension χ of the environment tensors C and E. In (d) the CTMRG transfer matrix $\mathcal{T}$, which is used to compute a correlation length ξ of $\rho(T)$ is shown. By grouping the three left and the three right indices of the transfer matrix into single indices, we obtain a matrix which we use to compute ξ (see Sec. VI). In (e) we define, analogously to (d), an operator o transfer matrix $\mathcal{T}_o$ which is used in the ξ extrapolation procedure (see Sec. VI). In (c)–(e) for simplicity we show CTMRG for the translationally invariant $|\Psi(T)\rangle$. Furthermore, we assume a translational-invariant state with tensor A being rotational and mirror symmetric.

Figs. 3(a)–3(c). Details of the algorithm can be found in Refs. [26,48].

VI. ξ EXTRAPOLATION

The correlation length ξ converges very slowly with increasing χ, unlike local observables, e.g., the energy or the magnetization [65,77]. Therefore, to determine the correlation length ξ of $|\psi(T)\rangle$ we use an extrapolation procedure from Ref. [77] which we summarize briefly below in the simplest case of a translationally invariant PEPS. The procedure uses the eigenvalues of the CTMRG transfer matrix $\mathcal{T}$ [see Fig. 3(d)].

To set up the extrapolation we define ϵ_j for each eigenvalue λ_j of $\mathcal{T}$,

$$\lambda_j/\lambda_0 = e^{-(\epsilon_j + i\phi_j)}, \tag{6}$$

where j numbers the eigenvalues of $\mathcal{T}$ ordered by the absolute value $|\lambda_0| \geqslant |\lambda_1| \geqslant |\lambda_2| \cdots$ and $\phi_j \in (-\pi, \pi]$ determines the phase of λ_j. A connected correlation function of a one-site operator o at a distance R is then expressed as

$$C_{oo}(R) = \langle o_0 o_R\rangle - \langle o_0\rangle\langle o_R\rangle = \sum_{j>0} f_j^{oo} e^{-(\epsilon_j + i\phi_j)R}. \tag{7}$$

Here, the form factors f_j^{oo} are defined as

$$f_j^{oo} = (\phi_0|\mathcal{T}_o|\phi_j)(\phi_j|\mathcal{T}_o|\phi_0), \tag{8}$$

$\mathcal{T}_o$ is a transfer matrix of the operator o shown in Fig. 3(e), and $|\phi_j)$, $(\phi_j|$ are left and right eigenvectors of $\mathcal{T}$ normalized as $(\phi_i|\phi_j) = \delta_{ij}$. Therefore, the correlation length obtained from $\mathcal{T}$ equals

$$\xi_{\mathcal{T}} = 1/\epsilon_1.$$

As the spectrum of $\mathcal{T}$ is continuous in the limit of $\chi \to \infty$, the extrapolation uses its deviation from continuity δ as a measure of finite-χ effects. To extrapolate we use eigenvalues of $\mathcal{T}$ contributing to a connected correlation function of the phase transition's order parameter $C^{mm}(R)$, i.e., the eigenvalues with nonzero form factors of the order parameter f_j^{mm}. We denote ϵ's of such eigenvalues by $\{\epsilon_k^{mm},\ k = 1, 2, \dots\}$ with $\epsilon_1^{mm} \leqslant \epsilon_2^{mm} \leqslant \cdots$. We remark that in the case of a second-order phase transition, the diverging ξ is associated with the symmetry breaking, so we expect that the leading eigenvalue of the transfer matrix determines the asymptotics of the order parameter correlation function, i.e., $\epsilon_1^{mm} = \epsilon_1$. We observe that this is indeed the case for the transitions investigated below. We note that λ_0 does not contribute to $C^{mm}(R)$ by definition. We define δ as a distance in-between two dominant ϵ_k^{mm}, i.e.,

$$\delta = \epsilon_2^{mm} - \epsilon_1^{mm}. \tag{9}$$

We note that this choice of δ was proposed and benchmarked in Ref. [77]. Using the spectra from different values of χ, we extrapolate ϵ_1^{mm} as a function of δ by fitting

$$\epsilon_1^{mm} = \epsilon_1^e + a\delta^b, \tag{10}$$

where ϵ_1^e is an extrapolated value of ϵ_1^{mm} and a, b are parameters of the fit. The extrapolation gives us

$$\xi = 1/\epsilon_1^e. \tag{11}$$

In Fig. 4 we present examples of the extrapolation for the quantum Ising model with parameters which are investigated later in Sec. IX.

VII. FINITE CORRELATION LENGTH SCALING

Finite correlation length scaling (FCLS) was introduced for simulations of 1D quantum critical phenomena [63,64,67] with infinite MPS. In this case, a finite iMPS bond dimension D introduces a finite correlation length ξ_D at a critical point. ξ_D

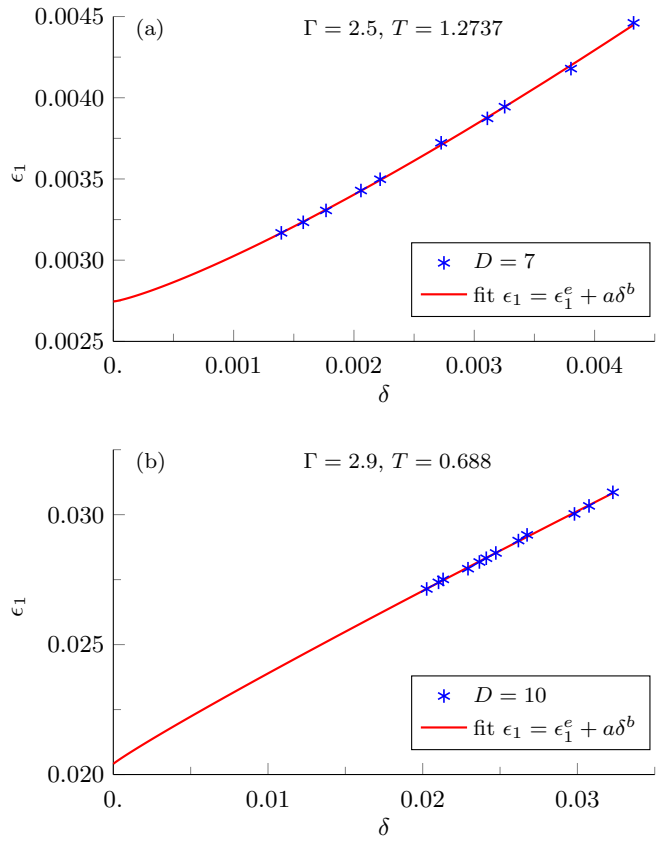

FIG. 4. Examples of the ξ extrapolation for the quantum Ising model in the vicinity of T_c. In (a) the case of $\Gamma = 2.5$ and $T = 1.2737$ simulated with $D = 7$ and $56 \geqslant \chi \geqslant 168$. The fit gives the extrapolated inverse ξ $\epsilon_1^e = 0.00275(10)$ and the exponent $b = 1.23(14)$. In (b), the extrapolation for $\Gamma = 2.9$ and $T = 0.6088$ simulated with $D = 10$ and $85 \geqslant \chi \geqslant 220$. Here, the fit gives $\epsilon_1^e = 0.020(3)$ and $b = 0.94(35)$.

acts as a cutoff on the diverging correlation length, similarly as a finite system size. It was shown that a scaling analysis in ξ_D can be done in a similar way as in conventional finite-size scaling, by replacing the system size L by ξ_D [63,64,67] in a scaling *Ansatz*, and then make use of this *Ansatz* to obtain the location of the critical point and the values of universal critical exponents. As the finite D introduces also a finite entanglement entropy at the critical point [68] FCLS for 1D critical phenomena was originally called finite entanglement scaling [63,64]. The FCLS was recently applied to iPEPS simulations of Lorentz-invariant quantum critical points [65,66] for which it was found that a finite D introduces finite ξ_D at the critical point [65].

Here, we consider a second-order finite-temperature phase transition for a quantum Hamiltonian. We use VTNR to find finite-D iPEPS approximating purifications of thermal states in the vicinity of the critical temperature T_c. We observe that the VTNR optimization introduces a finite correlation length ξ_D at $T = T_c$ [or equivalently at $t = (T - T_c)/T_c = 0$] for all D's reached in this work:

$$\xi(t = 0, D) = \xi_D. \tag{12}$$

This observation motivates us to consider an application of FCLS to obtain T_c and the critical exponents from the VTNR results.

We obtain the FCLS *Ansatz* for observables from the standard finite-size scaling *Ansatz* by replacing the finite system size by ξ_D, e.g., for the order parameter $m(t, D)$ we use

$$m(t, D) = \xi_D^{-\beta/\nu} \mathscr{M}\left(t\xi_D^{1/\nu}\right), \tag{13}$$

where β, ν are the critical exponents, and $\mathscr{M}$ is a nonuniversal function.

To compute observables we contract the iPEPS using CTMRG. The finite χ introduces an effective length scale ξ_χ [69], i.e., finite-χ values of the observables are given by a more complicated scaling *Ansatz* depending on both ξ_D and ξ_χ, e.g.,

$$m(t, D, \chi) = \xi_D^{-\beta/\nu} \bar{\mathscr{M}}\left(t\xi_D^{1/\nu}, \xi_D/\xi_\chi\right), \tag{14}$$

where $\bar{\mathscr{M}}$ is another nonuniversal function. To avoid working with the more complicated *Ansatz*, we work in the limit of $\chi \to \infty$ as proposed in Refs. [65,66]. We observe that there is no need to extrapolate the order parameter in χ as it converges quickly. On the other hand, to obtain a good estimate of $\xi(t, D) \equiv \xi(t, D, \chi \to \infty)$ we use the ξ extrapolation described in Sec. VI.

VIII. T_c ESTIMATION

Finite-size scaling usually makes use of the Binder cumulant to locate the critical point without prior knowledge of its critical exponents, but in the case of iPEPS computation of the Binder cumulant is challenging because the fourth-order moment of the order parameter would need to be computed. Instead, we apply the m'/m collapse introduced in [65], which makes use of the derivative of the order parameter $m'(t, D) = dm(t, D)/dt$, to find T_c. A FCLS scaling *Ansatz* for m' is

$$m'(t, D) = \xi_D^{-(\beta-1)/\nu} \mathscr{M}'\left(t\xi_D^{1/\nu}\right), \tag{15}$$

where $\mathscr{M}'$ is a nonuniversal function [65]. Using (13) and (15) we obtain

$$t\frac{m'(t, D)}{m(t, D)} = \bar{\mathscr{P}}\left(t\xi_D^{1/\nu}\right), \tag{16}$$

$$\xi_D^{1/\nu} \propto \frac{m'(t = 0, D)}{m(t = 0, D)}, \tag{17}$$

where $\bar{\mathscr{P}}$ is another nonuniversal function. Equations (16) and (17) give us the m'/m collapse

$$t\frac{m'(t, D)}{m(t, D)} = \mathscr{P}\left(t\frac{m'(t = 0, D)}{m(t = 0, D)}\right). \tag{18}$$

We estimate T_c by plotting $y = t\frac{m'(t,D)}{m(t,D)}$ versus $x = t\frac{m'(t=0,D)}{m(t=0,D)}$ for different choices of T_c and finding the one for which $y(x)$ data points obtained with different D collapse best onto a single curve.

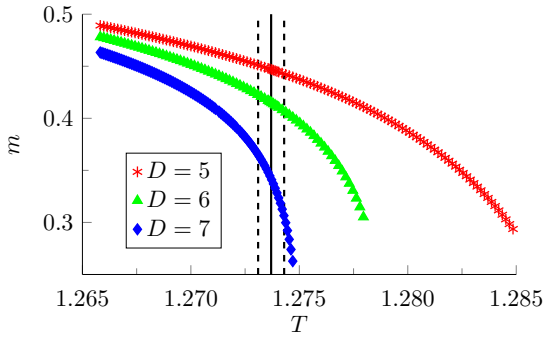

FIG. 5. The order parameter m in the vicinity of the critical temperature for the 2D quantum Ising model with $\Gamma = 2.5$ and $D = 5$–7. The critical behavior is smoothed out by finite-D effects. The black lines indicate the QMC estimate of the critical temperature $T_c = 1.2737(6)$ [79].

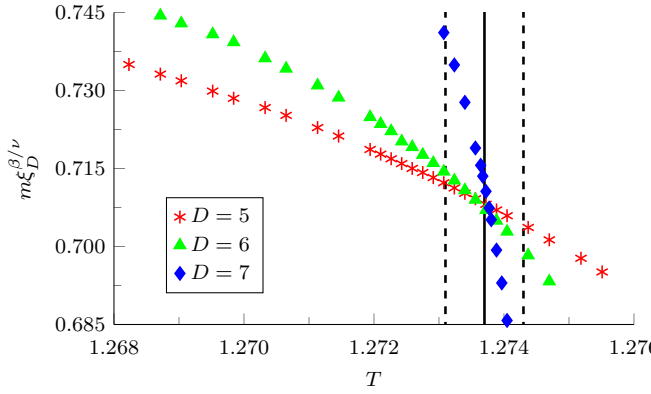

FIG. 6. T_c estimation for $\Gamma = 2.5$ by intersecting $m(T, D)\xi_D^{\beta/\nu}$ for different values of D [Eq. (21)]. Here, we assume the 2D classical Ising universality class with $\beta = \frac{1}{8}$ and $\nu = 1$. The $D = 5$–7 curves intersect, as predicted by FCLS, at $T_c = 1.2737(2)$ in agreement with the QMC estimate $T_c = 1.2737(6)$ [79], which is indicated by the black lines. Details of the T_c estimation can be found in the text.

IX. QUANTUM ISING MODEL: BENCHMARK RESULTS

The quantum Ising model is given by the Hamiltonian

$$H = -\sum_{\langle i,j\rangle} \sigma_z^i \sigma_z^j + \Gamma \sum_i \sigma_x^i, \tag{19}$$

where σ_z, σ_x are Pauli matrices. For $\Gamma = 0$ the model reduces to the classical Ising model with $T_c = 2/\ln(1+\sqrt{2}) \approx 2.269$ and for $\Gamma_c = 3.04438(2)$ [78] it has a quantum critical point. For $0 \leqslant \Gamma < \Gamma_c$ it exhibits a low-temperature ferromagnetic phase with the order parameter $m = \langle \sigma_z \rangle$, which is separated from the paramagnetic phase by a line of finite-temperature second-order phase transitions belonging to a 2D classical Ising universality class.

As Γ is approaching Γ_c, quantum fluctuations are becoming stronger and T_c gets suppressed with respect to the classical case of $\Gamma = 0$. Therefore, we expect that with increasing Γ the accurate simulation of the finite-temperature transition using tensor networks is becoming more challenging since a larger D is necessary to correctly capture the stronger quantum fluctuations. To examine this more closely, we investigate in the following $\Gamma = 2.5$ as well as a point close to the quantum critical point $\Gamma = 2.9$, for which quantum Monte Carlo (QMC) [79] gives $T_c = 1.2737(6)$ and $T_c = 0.6085(8)$, respectively, corresponding to a reduction in T_c with respect to $\Gamma = 0$ by a factor of 1.8 and 3.7, respectively.

A. $\Gamma = 2.5$

We first consider a case well away from the quantum critical point $\Gamma = 2.5$ to provide a proof of principle of the applicability of FCLS to finite-temperature VTNR simulations. In Fig. 5 we present data for the order parameter as a function of temperature in the vicinity of the critical temperature, for bond dimensions $D = 5$–7. As expected, we do not obtain a sharp phase transition but we see that the order parameter is systematically reduced with increasing D similarly to the case of finite-size effects.

We first attempt to estimate T_c by using the known critical exponents of the 2D classical Ising universality class, i.e., $\beta = \frac{1}{8}$ and $\nu = 1$. To do that we plot $m\xi_D^{\beta/\nu}$ which, according to FCLS, should not depend on D at $T = T_c$:

$$m(t, D)\xi_D^{\beta/\nu} = \mathscr{M}\left(t\xi_D^{1/\nu}\right), \tag{20}$$

$$m(t = 0, D)\xi_D^{\beta/\nu} = a, \tag{21}$$

where a does not depend on D. Indeed, the $m(t, D)\xi_D^{\beta/\nu}$ curves for different D's cross as predicted by FCLS (see Fig. 6). We identify T_c as the temperature for which the variance of $m(t, D)\xi_D^{\beta/\nu}$ is smallest, obtaining $T_c = 1.2737(2)$ in agreement with the QMC estimate $T_c = 1.2737(6)$ [79]. The T_c uncertainty is obtained by varying the range of D and the range of χ used for ξ_D estimation by extrapolation.

To provide further evidence of FCLS we determine the critical exponents, using $T_c = 1.2737(2)$ found earlier. We first estimate β/ν using the data obtained at $T = T_c$. From Eq. (21) we obtain

$$\log m(t = 0, D) = -\beta/\nu \log \xi_D + \log a. \tag{22}$$

A linear fit to the data on a log-log scale shown in Fig. 7(a) yields $\beta/\nu = 0.123(15)$, in agreement with the exact $\beta/\nu = \frac{1}{8}$. The error bar takes into account the T_c uncertainty and the statistical error of the fit.

Next, we estimate β and ν by performing data collapses based on data in the vicinity of T_c, using the scaling *Ansätze*:

$$m(t, D)\xi_D^{\beta/\nu} = \mathscr{M}\left(t\xi_D^{1/\nu}\right), \tag{23}$$

$$m(t, D)t^{-\beta} = \bar{\mathscr{M}}\left(t\xi_D^{1/\nu}\right). \tag{24}$$

Using the *Ansatz* (23) we obtain $\beta = 0.127(2)$, $\nu = 1.04(4)$, in agreement with the exact universality class [see Fig. 7(b)]. *Ansatz* (24) yields $\beta = 0.126(5)$, $\nu = 1.04(5)$, again in agreement with the exact exponents [see Fig. 7(c)]. In both cases, the uncertainties are obtained by taking into account the T_c uncertainty and by varying the data range.

Finally, we show that we can estimate T_c and β without prior knowledge of the universality class nor the value of T_c.

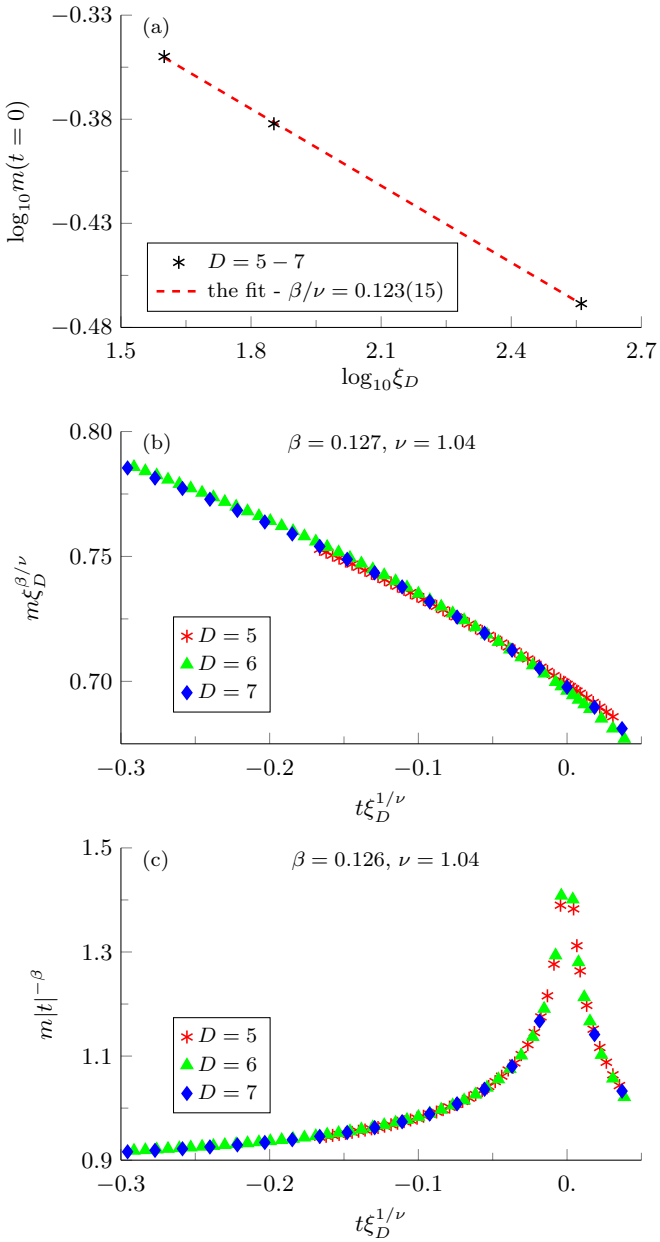

FIG. 7. Critical exponents estimation for $\Gamma = 2.5$, using $T_c = 1.2737(2)$ found earlier. In (a) a fit to Eq. (22) gives $\beta/\nu = 0.123(15)$, in agreement with the exact $\beta/\nu = \frac{1}{8}$. In (b) and (c), by performing data collapses using Eqs. (23) and (24) we obtain $\beta = 0.127(2)$, $\nu = 1.04(4)$ and $\beta = 0.126(5)$, $\nu = 1.04(5)$, respectively. The β and ν estimates agree with the exact $\beta = \frac{1}{8}$, $\nu = 1$.

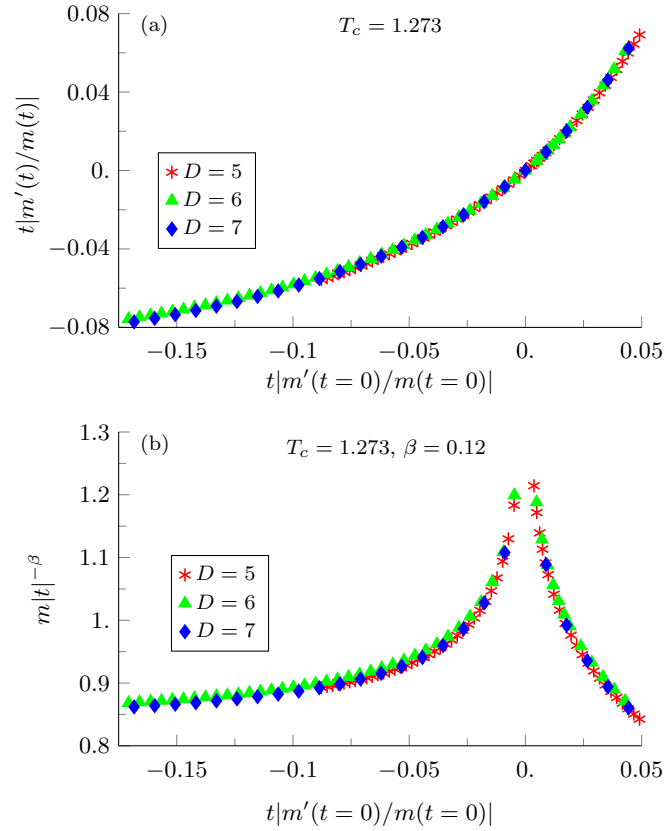

FIG. 8. T_c and β estimation for $\Gamma = 2.5$ without knowledge of the universality class nor the value of T_c. In (a) we use the m'/m *Ansatz* (18) to perform a data collapse, obtaining $T_c = 1.273(1)$. In (b) we estimate β by performing a data collapse based on Eq. (25), using the value of T_c found in (a), which yields $\beta = 0.12(1)$. The obtained T_c and β agree with the QMC estimate $T_c = 1.2737(6)$ [79] and the exact $\beta = \frac{1}{8}$.

First, we estimate T_c by performing a data collapse using the m'/m *Ansatz* (18), which yields $T_c = 1.273(1)$ [see Fig. 8(a)]. The T_c uncertainty is obtained by varying the data range. We estimate β by performing a data collapse based on the *Ansatz*

$$m(t, D)t^{-\beta} = \bar{\mathscr{P}}\left(t\frac{m'(t=0, D)}{m(t=0, D)}\right), \tag{25}$$

using for T_c the value obtained in the m'/m collapse. We obtain $\beta = 0.12(1)$ [see Fig. 8(b)]. The uncertainty is obtained taking into account the T_c uncertainty and varying the data range.

We remark that while the quality of the obtained results is good, we see some deviations from perfect scaling which may be caused either by corrections to finite-size scaling or limitations of VTNR in getting optimal tensors. First, we note that VTNR is not guaranteed to give the best iPEPS approximation of the thermal state's purification for a given D, as it does not search directly for the best iPEPS tensor representing thermal state purification. Instead, it optimizes a tree tensor network (TTN) of isometries which, applied to virtual indices of the tensor network representing a Suzuki-Trotter decomposition of the purification, gives the iPEPS approximating the purification. While this approach makes the variational optimization of the iPEPS efficient, it is not equivalent to the most general iPEPS variational optimization procedure. Still, our results demonstrate that the accuracy of the optimized tensors is high enough to extract the critical coupling and critical exponents with a good accuracy.

Second, we note that for $\Gamma = 2.5$ CTMRG convergence is challenging, as for $D = 5$–7 we obtain $\xi_{D=7} \sim 350$. For an iPEPS with such a large ξ many iterations of the CTMRG procedure are necessary to converge m. Good convergence

of the CTMRG environment is important for the variational optimization since VTNR uses the CTMRG environmental tensors to find the best iPEPS.[1] Here, to optimize the iPEPS we use $\chi = 8D$. We check that using $\chi = 6D$ and $\chi = 7D$ we obtain results [T_c and β obtained by the m'/m collapse and collapse (25)] in agreement with the ones obtained with $\chi = 8D$. Nevertheless, we cannot fully exclude the possibility that finite-χ effects contribute to the observed small deviations from the perfect collapse as simulations with larger χ would be computationally very expensive.

To obtain ξ_D we contract the final iPEPS with $8D \leqslant \chi \leqslant 24D$ and use the extrapolation procedure described in Sec. VI. We remark that in the case of VTNR simulations obtaining convergence in the small Trotter time step $\delta\tau$ is relatively easy as the computational cost of the simulations scales at most as $O[\log(1/\delta\tau)]$. For $\Gamma = 2.5$ we use a second-order Trotter decomposition with $\delta\tau = \tau/2^{10} \leqslant 0.001$, which is small enough to give results converged in $\delta\tau$.

B. $\Gamma = 2.9$

For the more challenging $\Gamma = 2.9$ case we analyze VTNR results for $D = 7$–10 [see Fig. 9(a)]. Using the m'/m collapse we obtain $T_c = 0.609(4)$ [see Fig. 9(b)]. Using this result for T_c and performing a collapse with Eq. (25) we obtain $\beta = 0.152(8)$ [see Fig. 9(c)]. While the obtained T_c estimate agrees with the QMC estimate $T_c = 0.6085(8)$ [79], the β estimate deviates by about 20% from the exact $\beta = \frac{1}{8}$.

Comparing the results obtained with $D = 8$–10 and $D = 7$–10 suggests that the β estimate still depends significantly on the D range as we obtain $\beta = 0.145(5)$ for $D = 8$–10.[2] Furthermore, we expect that the necessary ξ_D to obtain the asymptotic scaling is larger for $\Gamma = 2.9$ than for $\Gamma = 2.5$, as $\Gamma = 2.9$ is closer to the quantum critical point. Despite larger D, the ξ_D obtained for $\Gamma = 2.9$, although quite large ($\xi_D \sim 20$–50), is smaller than ξ_D for $\Gamma = 2.5$ ($\xi_D \sim 40$–350). Therefore, we expect that the quality of the results can still be improved by increasing D, although it would be computationally very expensive.

The T_c and β uncertainties are estimated in the same way as in the $\Gamma = 2.5$ case. Similar values for T_c and β are obtained with VTNR using an optimization with $\chi = 5D, 6D, 7D$. A second-order Trotter decomposition with a time step $\delta\tau = \tau/2^{10} \leqslant 0.002$ is used.

X. INTERACTING HONEYCOMB FERMIONS: BENCHMARK RESULTS

We consider a model of interacting spinless fermions on a honeycomb lattice [80], given by the Hamiltonian

$$H = -t \sum_{\langle i,j \rangle} (c_i^\dagger c_j + c_j^\dagger c_i) + V \sum_{\langle i,j \rangle} n_i n_j. \tag{26}$$

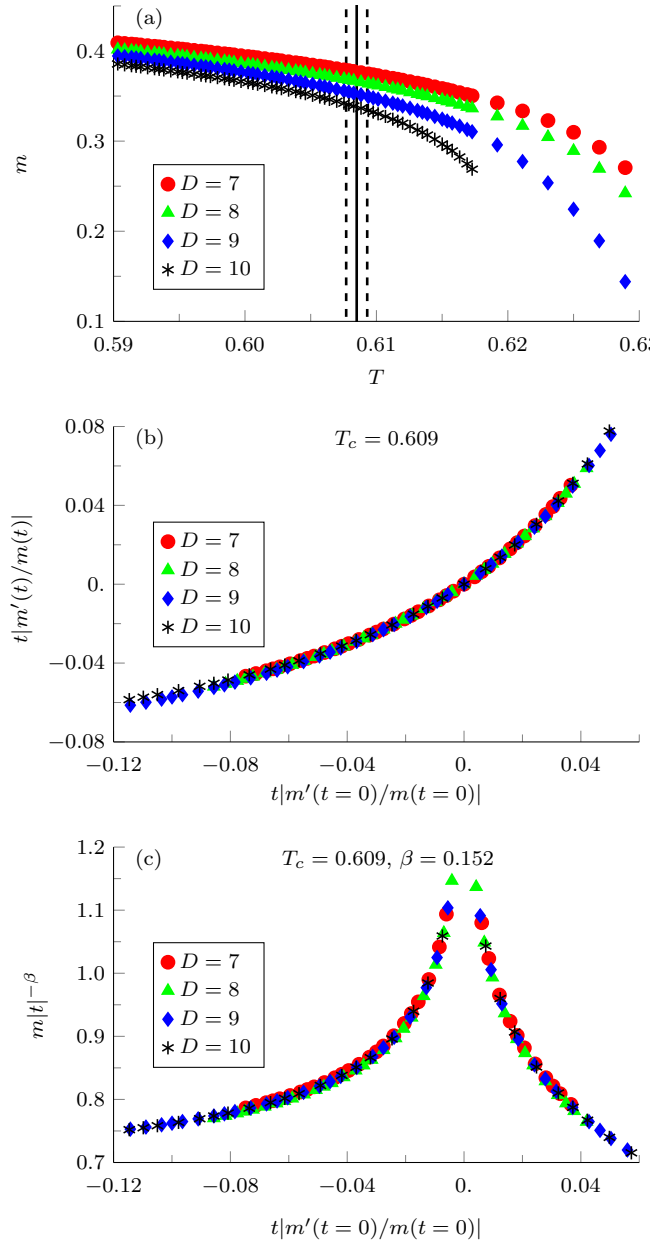

FIG. 9. Results for the more challenging $\Gamma = 2.9$ case. In (a) the order parameter in the vicinity of T_c for $D = 7$–10. The black lines indicate the QMC estimate $T_c = 0.6085(8)$ [79]. In (b) the m'/m collapse (18) gives $T_c = 0.609(4)$. In (c) β estimation based on a data collapse using Eq. (25) and taking T_c found in (b) gives $\beta = 0.152(8)$. The obtained T_c agrees with QMC, but the obtained β deviates from the exact one $\beta = \frac{1}{8}$ by about 20% (see main text for a discussion of this deviation).

Here, c_i ($c_i^\dagger$) is a fermionic annihilation (creation) operator at site i and $n_i = c_i^\dagger c_i$ is a fermion number operator. We set $t = 1$ in the following. Furthermore, for the purpose of the benchmark we restrict ourselves to the case of half-filling, $n = \sum_{i=1}^{N} \langle n_i \rangle / N = \frac{1}{2}$, for which sign-problem free QMC results are available [79,81,82]. The model has a quantum critical point at $V_c = 1.356(1)$ [81]. For $V > V_c$ there is a low-temperature phase with a charge density wave (CDW) order,

[1] To ensure a good CTMRG convergence, we require the change of m per CTMRG iteration to be smaller than 10^{-8}.

[2] Contrary to the case of β, the T_c estimate for $D = 8$–10, $T_c = 0.610(4)$, is similar to the $D = 7$–10 estimate.

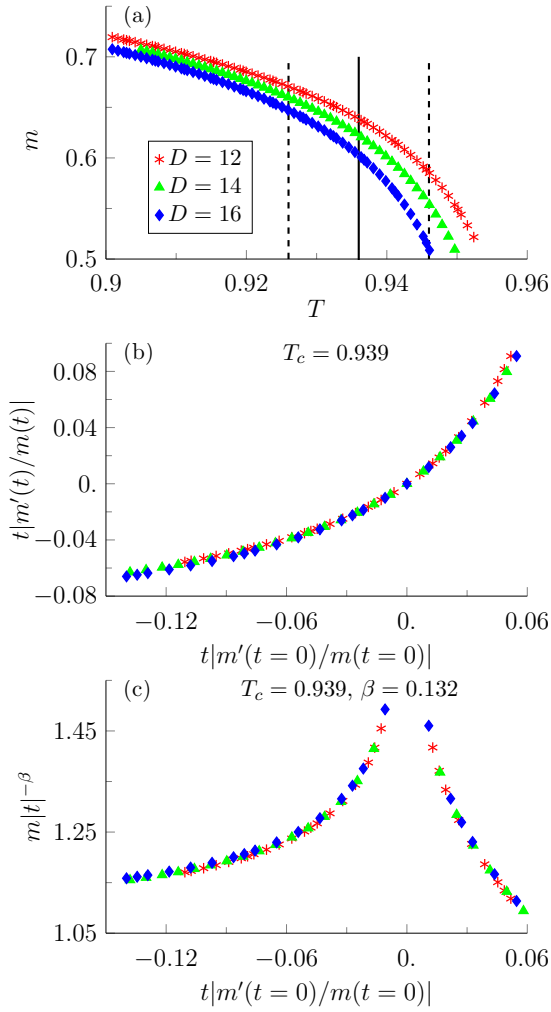

FIG. 10. Results for the spinless honeycomb fermion model (26) with $V = 3$. In (a) the order parameter close to T_c for $D = 12, 14, 16$ is shown. The black lines indicate the QMC estimate $T_c = 0.936(10)$ [79]. In (b) T_c is estimated by the m'/m collapse giving $T_c = 0.939(4)$ in agreement with QMC. In (c) a collapse using Eq. (25) yields $\beta = 0.132(8)$ using T_c found in (b). The obtained β agrees with the exact $\beta = \frac{1}{8}$.

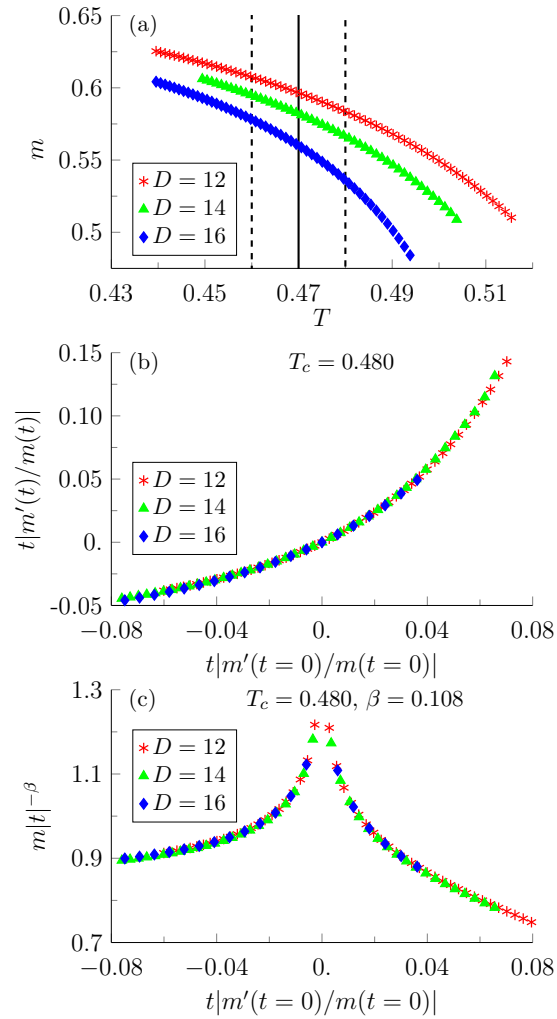

FIG. 11. Results for the more challenging $V = 2$ case. In (a) the order parameter close to T_c for $D = 12, 14, 16$ is shown. The black lines indicate the QMC estimate $T_c = 0.47(1)$ [79]. In (b) the m'/m data collapse gives $T_c = 0.480(5)$ in agreement with QMC. In (c) a data collapse using Eq. (25) yields $\beta = 0.108(4)$ using T_c found in (b). The obtained β differs from the exact $\beta = \frac{1}{8}$ by about 10%. A discussion of the deviation in β can be found in the main text.

which is separated from a disordered, high-temperature, phase by a line of second-order finite-temperature phase transitions, which belong to the 2D classical Ising universality class [82]. The CDW order parameter is defined as

$$m = \langle n_A \rangle - \langle n_B \rangle, \tag{27}$$

where $\langle n_A \rangle$ and $\langle n_B \rangle$ are the fermion densities on sub-lattices A and B, respectively. In the limit of $V \to \infty$ the model becomes equivalent to the 2D classical antiferromagnetic Ising model. Here, we simulate the model for $V = 3$ and the more challenging case of $V = 2$, which is closer to V_c.

A. $V = 3$

For $V = 3$ we analyze $D = 12, 14, 16$ VTNR results in the vicinity of T_c [see Fig. 10(a)]. Here, QMC predicts $T_c = 0.936(10)$ [79]. We determine T_c using the m'/m collapse obtaining $T_c = 0.939(4)$ in agreement with QMC [see Fig. 10(b)]. Furthermore, we obtain $\beta = 0.132(8)$ in agreement with the exact $\beta = \frac{1}{8}$ by performing a data collapse using Eq. (25) and by taking T_c obtained from the m'/m collapse [see Fig. 10(c)].

The T_c and β uncertainties are obtained similarly as for the quantum Ising model. We use $\chi = 5D$ to perform the VTNR optimization obtaining results which are consistent with the ones obtained with $\chi = 3D$ and $\chi = 4D$. We use a second-order Suzuki-Trotter decomposition with a time step $\delta\tau = \tau/2^{11} < 0.001$.

B. $V = 2$

Next, we analyze $D = 12, 14, 16$ VTNR results for the more challenging $V = 2$ case [see Fig. 11(a)]. Using the m'/m collapse we obtain $T_c = 0.480(5)$ in agreement with the QMC

estimate $T_c = 0.47(1)$ [79] [see Fig. 11(b)]. Using *Ansatz* (25) and taking T_c found by the m'/m collapse, we obtain $\beta = 0.108(4)$ [see Fig. 11(c)]. The β estimate deviates by about 10% from the exact $\beta = \frac{1}{8}$. We see that the obtained ξ_D for $V = 2$ ($\xi_D \sim 2$–4) is much smaller than ξ_D for $V = 3$ ($\xi_D \sim 10$–20). Furthermore, as $V = 2$ is closer to the quantum critical point than $V = 3$ we expect that for $V = 2$, a larger ξ_D is necessary to be in the asymptotic scaling regime and we expect that the accuracy of β can be improved by increasing D.

The T_c and β uncertainties are obtained similarly as for the quantum Ising model. Here, we use $\chi = 5D$ to perform the VTNR optimization. Consistent results are obtained also with $\chi = 3D$ and $4D$. We use a second-order Suzuki-Trotter decomposition with a time step $\delta\tau = \tau/2^8 < 0.01$.

XI. CONCLUSIONS

In this paper we have studied second-order finite-temperature phase transitions in the 2D quantum Ising [Eq. (19)] and interacting honeycomb fermion [Eq. (26)] models using infinite projected entangled pair states (iPEPS) to represent thermal states. The iPEPS were obtained by variational tensor network renormalization (VTNR). We found that at the critical temperature T_c, the iPEPS correlation length ξ_D is finite for the computationally accessible values of the iPEPS bond dimension D. Motivated by this observation, we investigated the application of finite correlation length scaling (FCLS) to obtain precise values of T_c and universal critical exponents. We found that in the vicinity of T_c, the order parameter obeys well the expected behavior predicted by FCLS.

The two models studied in this work exhibit second-order finite-temperature phase transitions for the transverse fields $\Gamma < \Gamma_c \approx 3.044\,38$ and the interaction strengths $V > V_c \approx 1.356$, respectively. At Γ_c and V_c, second-order quantum phase transitions occur at $T = 0$. Using FCLS we obtained estimates of T_c and the critical exponents in agreement with the QMC results for $\Gamma = 2.5$ and $V = 3$ which are sufficiently far from the quantum critical points. For Γ and V approaching the quantum critical points, we observed that the magnitude of ξ_D and the accuracy of the critical data become lower for the same values of D. Nevertheless, we were still able to obtain T_c in agreement with the QMC results for the challenging $\Gamma = 2.9$ and $V = 2$ cases. For these couplings, the values of the critical exponents exhibit a dependence on the range of D values used in the scaling analysis, suggesting that larger D's are needed in order to obtain more accurate estimates of the critical exponents.

In summary, our results further demonstrate the usefulness of tensor network simulations for quantum many-body systems at finite temperature, even for the challenging case of a finite-temperature continuous phase transition, for which convergence in D can typically not be reached, but which can be systematically studied using FCLS.

ACKNOWLEDGMENTS

We thank S. Hesselmann and S. Wessel for providing us numerical values of data published in Ref. [79] and M. Rams for useful remarks about the manuscript. This research was funded by the National Science Centre (NCN), Poland, under Project No. 2016/23/B/ST3/00830 and the European Research Council (ERC) under the EU Horizon 2020 research and innovation program (Grant Agreement No. 677061).

[1] F. Verstraete, V. Murg, and J. Cirac, Adv. Phys. **57**, 143 (2008).
[2] U. Schöllwock, Ann. Phys. (NY) **326**, 96 (2011).
[3] R. Orús, Ann. Phys. (NY) **349**, 117 (2014).
[4] J. C. Bridgeman and C. T. Chubb, J. Phys. A: Math. Theor. **50**, 223001 (2017).
[5] R. Orus, arXiv:1812.04011.
[6] M. B. Hastings, J. Stat. Mech. (2007) P08024.
[7] J. Eisert, M. Cramer, and M. B. Plenio, Rev. Mod. Phys. **82**, 277 (2010).
[8] N. Laflorencie, Phys. Rep. **646**, 1 (2016).
[9] C. Pineda, T. Barthel, and J. Eisert, Phys. Rev. A **81**, 050303(R) (2010).
[10] P. Corboz, G. Evenbly, F. Verstraete, and G. Vidal, Phys. Rev. A **81**, 010303(R) (2010).
[11] P. Corboz and G. Vidal, Phys. Rev. B **80**, 165129 (2009).
[12] C. V. Kraus, N. Schuch, F. Verstraete, and J. I. Cirac, Phys. Rev. A **81**, 052338 (2010).
[13] T. Barthel, C. Pineda, and J. Eisert, Phys. Rev. A **80**, 042333 (2009).
[14] P. Corboz, R. Orús, B. Bauer, and G. Vidal, Phys. Rev. B **81**, 165104 (2010).
[15] S. R. White, Phys. Rev. Lett. **69**, 2863 (1992).
[16] S. R. White, Phys. Rev. B **48**, 10345 (1993).
[17] I. Affleck, T. Kennedy, E. H. Lieb, and H. Tasaki, Phys. Rev. Lett. **59**, 799 (1987).
[18] M. Fannes, B. Nachtergaele, and R. F. Werner, Commun. Math. Phys. **144**, 443 (1992).
[19] S. Östlund and S. Rommer, Phys. Rev. Lett. **75**, 3537 (1995).
[20] F. Verstraete and J. I. Cirac, arXiv:cond-mat/0407066.
[21] T. Nishino, Y. Hieida, K. Okunishi, N. Maeshima, Y. Akutsu, and A. Gendiar, Prog. Theor. Phys. **105**, 409 (2001).
[22] Y. Nishio, N. Maeshima, A. Gendiar, and T. Nishino, arXiv:0401115.
[23] V. Murg, F. Verstraete, and J. I. Cirac, Phys. Rev. A **75**, 033605 (2007).
[24] J. Jordan, R. Orús, G. Vidal, F. Verstraete, and J. I. Cirac, Phys. Rev. Lett. **101**, 250602 (2008).
[25] H. C. Jiang, Z. Y. Weng, and T. Xiang, Phys. Rev. Lett. **101**, 090603 (2008).
[26] P. Corboz, T. M. Rice, and M. Troyer, Phys. Rev. Lett. **113**, 046402 (2014).
[27] B.-X. Zheng, C.-M. Chung, P. Corboz, G. Ehlers, M.-P. Qin, R. M. Noack, H. Shi, S. R. White, S. Zhang, and G. K.-L. Chan, Science **358**, 1155 (2017).

[28] Z. Y. Xie, J. Chen, J. F. Yu, X. Kong, B. Normand, and T. Xiang, Phys. Rev. X **4**, 011025 (2014).
[29] H. J. Liao, Z. Y. Xie, J. Chen, Z. Y. Liu, H. D. Xie, R. Z. Huang, B. Normand, and T. Xiang, Phys. Rev. Lett. **118**, 137202 (2017).
[30] D. Poilblanc and M. Mambrini, Phys. Rev. B **96**, 014414 (2017).
[31] R. Haghshenas and D. N. Sheng, Phys. Rev. B **97**, 174408 (2018).
[32] P. Corboz and F. Mila, Phys. Rev. Lett. **112**, 147203 (2014).
[33] A. Kshetrimayum, H. Weimer, and R. Orús, Nat. Commun. **8**, 1291 (2017).
[34] L. Vanderstraeten, J. Haegeman, and F. Verstraete, Phys. Rev. B **99**, 165121 (2019).
[35] D. M. Kennes, arXiv:1811.04126.
[36] P. Czarnik, J. Dziarmaga, and P. Corboz, Phys. Rev. B **99**, 035115 (2019).
[37] C. Hubig and J. I. Cirac, SciPost Phys. **6**, 31 (2019).
[38] M. Lubasch, J. I. Cirac, and M.-C. Bañuls, Phys. Rev. B **90**, 064425 (2014).
[39] H. N. Phien, J. A. Bengua, H. D. Tuan, P. Corboz, and R. Orús, Phys. Rev. B **92**, 035142 (2015).
[40] P. Corboz, Phys. Rev. B **94**, 035133 (2016).
[41] L. Vanderstraeten, J. Haegeman, P. Corboz, and F. Verstraete, Phys. Rev. B **94**, 155123 (2016).
[42] Z. Y. Xie, H. J. Liao, R. Z. Huang, H. D. Xie, J. Chen, Z. Y. Liu, and T. Xiang, Phys. Rev. B **96**, 045128 (2017).
[43] M. T. Fishman, L. Vanderstraeten, V. Zauner-Stauber, J. Haegeman, and F. Verstraete, Phys. Rev. B **98**, 235148 (2018).
[44] M. M. Wolf, F. Verstraete, M. B. Hastings, and J. I. Cirac, Phys. Rev. Lett. **100**, 070502 (2008).
[45] P. Czarnik, L. Cincio, and J. Dziarmaga, Phys. Rev. B **86**, 245101 (2012).
[46] P. Czarnik and J. Dziarmaga, Phys. Rev. B **90**, 035144 (2014).
[47] P. Czarnik and J. Dziarmaga, Phys. Rev. B **92**, 035152 (2015).
[48] P. Czarnik, M. M. Rams, and J. Dziarmaga, Phys. Rev. B **94**, 235142 (2016).
[49] P. Czarnik and J. Dziarmaga, Phys. Rev. B **98**, 045110 (2018).
[50] A. Kshetrimayum, M. Rizzi, J. Eisert, and R. Orús, Phys. Rev. Lett. **122**, 070502 (2019).
[51] Z.-C. Gu, M. Levin, and X.-G. Wen, Phys. Rev. B **78**, 205116 (2008).
[52] W. Li, S.-J. Ran, S.-S. Gong, Y. Zhao, B. Xi, F. Ye, and G. Su, Phys. Rev. Lett. **106**, 127202 (2011).
[53] Z. Y. Xie, J. Chen, M. P. Qin, J. W. Zhu, L. P. Yang, and T. Xiang, Phys. Rev. B **86**, 045139 (2012).
[54] S.-J. Ran, W. Li, B. Xi, Z. Zhang, and G. Su, Phys. Rev. B **86**, 134429 (2012).
[55] S.-J. Ran, B. Xi, T. Liu, and G. Su, Phys. Rev. B **88**, 064407 (2013).
[56] B. Bruognolo, Z. Zhu, S. R. White, and E. M. Stoudenmire, arXiv:1705.05578.
[57] B.-B. Chen, L. Chen, Z. Chen, W. Li, and A. Weichselbaum, Phys. Rev. X **8**, 031082 (2018).
[58] C. Peng, S.-J. Ran, T. Liu, X. Chen, and G. Su, Phys. Rev. B **95**, 075140 (2017).
[59] P. Czarnik, J. Dziarmaga, and A. M. Oleś, Phys. Rev. B **96**, 014420 (2017).
[60] S.-J. Ran, W. Li, S.-S. Gong, A. Weichselbaum, J. von Delft, and G. Su, Phys. Rev. B **97**, 075146 (2018).
[61] X. Chen, S.-J. Ran, T. Liu, C. Peng, Y.-Z. Huang, and G. Su, Sci. Bull. **63**, 1545 (2018).
[62] L. Chen, D.-W. Qu, H. Li, B.-B. Chen, S.-S. Gong, J. von Delft, A. Weichselbaum, and W. Li, Phys. Rev. B **99**, 140404 (2019).
[63] L. Tagliacozzo, T. R. de Oliveira, S. Iblisdir, and J. I. Latorre, Phys. Rev. B **78**, 024410 (2008).
[64] F. Pollmann, S. Mukerjee, A. M. Turner, and J. E. Moore, Phys. Rev. Lett. **102**, 255701 (2009).
[65] P. Corboz, P. Czarnik, G. Kapteijns, and L. Tagliacozzo, Phys. Rev. X **8**, 031031 (2018).
[66] M. Rader and A. M. Läuchli, Phys. Rev. X **8**, 031030 (2018).
[67] B. Pirvu, G. Vidal, F. Verstraete, and L. Tagliacozzo, Phys. Rev. B **86**, 075117 (2012).
[68] G. Vidal, J. I. Latorre, E. Rico, and A. Kitaev, Phys. Rev. Lett. **90**, 227902 (2003).
[69] T. Nishino, K. Okunishi, and M. Kikuchi, Phys. Lett. A **213**, 69 (1996).
[70] H. F. Trotter, Proc. Am. Math. Soc. **10**, 545 (1959).
[71] M. Suzuki, J. Phys. Soc. Jpn. **21**, 2274 (1966).
[72] M. Suzuki, Prog. Theor. Phys. **56**, 1454 (1976).
[73] L. Tagliacozzo, G. Evenbly, and G. Vidal, Phys. Rev. B **80**, 235127 (2009).
[74] R. J. Baxter, J. Stat. Phys. **19**, 461 (1978).
[75] T. Nishino and K. Okunishi, J. Phys. Soc. Jpn. **65**, 891 (1996).
[76] R. Orús and G. Vidal, Phys. Rev. B **80**, 094403 (2009).
[77] M. M. Rams, P. Czarnik, and L. Cincio, Phys. Rev. X **8**, 041033 (2018).
[78] H. W. J. Blöte and Y. Deng, Phys. Rev. E **66**, 066110 (2002).
[79] S. Hesselmann and S. Wessel, Phys. Rev. B **93**, 155157 (2016).
[80] S. Capponi, J. Phys.: Condens. Matter **29**, 043002 (2017).
[81] L. Wang, P. Corboz, and M. Troyer, New J. Phys. **16**, 103008 (2014).
[82] L. Wang, Y.-H. Liu, and M. Troyer, Phys. Rev. B **93**, 155117 (2016).